Demonstration of a transformer-coupled field-effect transistor as a cryogenic pre-amplifier for frequency-domain readout of transition-edge sensor bolometers

Maclean Rouble
Department of Physics, McGill University
Montreal, Quebec
August, 2020

A thesis submitted to McGill University in partial fulfillment of the requirements of the degree of

Master of Physics

August 31, 2020

Abstract

Imaging the sky at millimeter wavelengths has, over the last half-century, contributed richly to our understanding of the nature and evolution of the universe, with such valuable prizes still to be found as the miniscule polarization signature left by a period of cosmic inflation. As future experiments seek to detect ever fainter signals, they require ever higher sensitivities. Modern detector and readout technologies regularly achieve photon-noise-limited levels of performance; consequently, improvements are to be made by increasing the number of detectors performing measurements, rather than by improving the individual performance of each. Operation of such high numbers of detectors is done through multiplexing, where the signals of multiple detectors are read out on a single amplifier chain, typically with the front end of this chain being a superconducting quantum interference device (SQUID). While SQUID amplifiers achieve excellent performance in terms of noise, transimpedance, and input impedance, they present several practical challenges in operation, particularly in their linearity. In this thesis, a prototype cryogenic pre-amplifier for frequency-multiplexed (fMUX) readout systems is described and characterized, which seeks to match the performance of existing SQUID-based fMUX systems, while providing a dramatically broadened linear operating range and a decreased overall complexity. This system couples a high-turns-ratio, wideband cryogenic transformer to a traditional, high-linearity, high-dynamic-range field-effect transistor amplifier in a novel low-impedance topology, to achieve frequency-multiplexed signal readout over a bandwidth of 1 to 6MHz, with a transimpedance of 267 $\pm 2\Omega$, input impedance of $\sim 0.2\Omega$, and system noise of 16$\pm$3 pA/$\sqrt{\mathrm{Hz}}$, comparable to that of existing SQUID-based fMUX systems.

Abrg

L'imagerie du ciel à des longueurs d'onde millimétriques a, au cours du dernier demi-siècle, grandement contribué à notre compréhension de la nature et de l'évolution de l'univers, et il reste des prix aussi precieux à y trouver, parmi eux la signature miniscule de polarisation laissée par une période de inflation cosmique. Alors que les expériences futures cherchent à détecter des signaux toujours plus faibles, elles nécessitent des sensibilités toujours plus élevées. Les technologies modernes de détection et de lecture atteignent régulièrement des niveaux de performances limités par le bruit des photons; par conséquent, des améliorations doivent être apportées en augmentant le nombre de détecteurs effectuant des mesures, plutôt qu'en améliorant les performances individuelles de chacun. Le fonctionnement d'un nombre si élevé de détecteurs se fait par multiplexage, où les signaux de plusieurs détecteurs sont lus sur une seule chaîne d'amplificateur, généralement avec le premier stage de cette chaîne un magnétomètre d'interférence quantique supraconducteur (SQUID). Bien que les amplificateurs SQUID atteignent d'excellentes performances en termes de bruit, de transimpédance et d'impédance d'entrée, ils présentent plusieurs défis pratiques en fonctionnement, en particulier dans leur linéarité. Dans cette thèse, un préamplificateur prototype cryogénique pour des systmes de lecture à multiplexage en fréquence (fMUX) est décrit et caractérisé, qui cherche à faire correspondre les performances des systèmes fMUX basés sur des SQUID existants, tout en fournissant un plage de fonctionnement linéaire considérablement élargie et un complexité globale réduite. Ce système associe un transformateur cryogénique à large bande et rapport de tours élevé à un amplificateur à transistor à effet de champ (FET) traditionnel haute linéarité et haute gamme dynamique dans une nouvelle topologie à faible impédance, pour obtenir une lecture du signal multiplexée en fréquence sur une bande passante de 1 à 6 MHz, avec une transimpédance de 267 $\pm 2\Omega$, une impédance d'entrée de $\sim 0,2\Omega$ et un bruit système de 16 $\pm$3 pA $/\sqrt{\mathrm{Hz}}$, comparable à celui des systèmes fMUX SQUID existants.

Acknowledgements

This work would not have been possible without contributions from many others. Firstly, from Clara Vergès, whose initial construction and characterization of the transformer and prototype system laid a groundwork that I have relied heavily upon. From Adam Gilbert, who with enthusiasm and/or patience, fielded my multitude of electronics questions and provided insights that I would not have found on my own. From Eamon Egan, whose depth of electrical engineering expertise has been invaluable in finessing our understanding of our prototype systems, and whose meticulous characterization of the test transformer cores was essential. From my labmates, Gavin Noble and Joshua Montgomery, who showed me the ropes, helped me through early cryogenic tribulations, and worked with me late into many nights. Finally, from my supervisor, Matt Dobbs, whose vision and guidance got this project off the ground, whose feedback (particulary in the last month) has always been timely and insightful, and whose coffee-machine chats have provided both laughter and inspiration.

Table of Contents

List of Figures

List of Tables

Chapter 1

Introduction

In the nearly six decades since its detection, the cosmic microwave background (CMB) has proven to hold significant insights to the nature of matter and the universe. This relic light, left over from the end of the radiation-opaque universe, is perfusive across the sky, nearly even in its distribution in all directions. Looking out at it with increasing levels of detail and study has, over the years, yielded significant reward to the furtherment of our understanding of the laws of nature, from cosmology to particle physics. Likewise, these advances have been made possible by increasing performance in CMB measurement technology and instrumentation.

1.1 Current state of the art

At present, entering the second decade of the millenium, many questions have both arisen from and been answered by studies of the CMB. Beginning with the fundamental questions of its source – not the scattered starlight of distant galaxies as initially proposed but instead a perfect thermal black body, already pointing to an origin that disagreed firmly with the model of a steady-state universe – it has continued to yield groundbreaking insights into many aspects of the field of physics as a whole.

Present studies focus intently on the details of its anisotropies. With the predictions in the 1970s of inhomogeneities in the early universe [1][2][3], and in turn the prediction of the imprints of these inhomogeneities on the CMB[4], the search was on. Narrowing constraints on the scale of the anisotropy throughout the following several decades culminated in the detection of the primary anistropy by the Nobel Prize-winning 1992 COBE mission results [5], confirming the presence of inhomogeneities at the surface of last scattering.

Following in the footsteps of COBE's Differential Microwave Radiometer instrument, the development of increasingly sensitive experiments has yielded increasingly detailed views of the CMB anisotropy. At large scales, the coherence of these inhomogeneities is wider than the cosmological horizon, necessitating either a belief in delicate fine-tuning of the state of the universe, or the introduction of additional theories of physics in the very early universe, such as cosmic inflation.

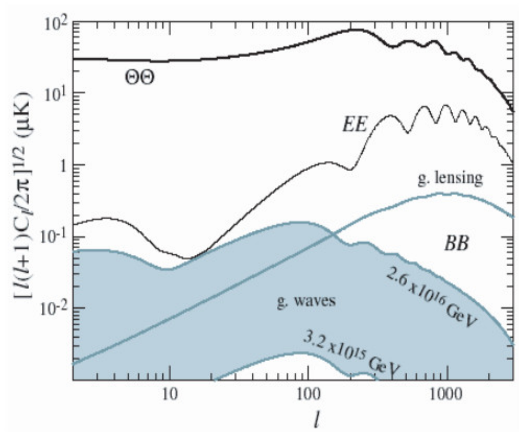

Figure 1.1: Predicted spectra for temperature (ΘΘ) and polarization (E-mode EE, B-mode BB). The spread in BB is shown for primordial gravitational waves, corresponding to a range of energy scales in inflation, and the dominant component at high l is indicated for B-mode polarization incurred via lensing. Figure from Trevor Lanting's PhD thesis, [13].

At present, the anisotropy in the temperature of the CMB has been measured repeatedly by a range of experiments to a great level of precision [6][7][8][9][10][11], and experiments now look to investigate its polarization. While fluctuations in its temperature are on the order of 10^{-4} or 10^{-5}, fluctuations in its polarization range in size from one to two orders smaller [12], necessitating a much finer level of detail to resolve.

1.2 Polarization

Providing two direct observables—curl-free E modes and divergence-free B modes—which, along with temperature, yield a total of six measurables via cross-correlation, the polarization of the CMB holds the promise of being able to observationally constrain models of the nature and generation mechanism of perturbations in the very early universe. Existing in three modes, scalar, vector, and tensor, each with a geometrically distinct source, these perturbations imparted a polarization onto the photons that would make up the CMB as they were scattered a final time. As this scattering process is inherently quick, their polarization provides a snapshot of the local state of the primordial plasma along the surface of last scattering, at a well-defined epoch. Scalar perturbations drive density disparities, leading to the temperature anisotropy seen in the CMB today and its corresponding E-mode polarization. Vector mode perturbations represent vortical motion, which is damped over time by the expansion of the universe, and so are expected to be negligible. Tensor perturbations are quadrupolar distortions of the metric, as created by passing gravitational waves, and produce both E and B modes.

As is the case for temperature anisotropy in the CMB, a useful representation of the anisotropy in its polarization is its power spectrum. Obtained by detailed surveys of patches of sky over a range of sizes, these spectra represent the strength of the anisotropy in each polarization mode at a given angular scale (or more conveniently, in terms of the corresponding multipole moment, l). Predictions for such power spectra are shown in Figure 1.1, where the uppermost heavy line $\Theta\Theta$ indicates the temperature anisotropy, the subsequent EE line indicates the E-mode polarization, the third line indicates the B-mode spectrum from gravitational lensing, and the lowermost shaded region depicts a range of cosmological B-mode spectra.

Though intervening dust and matter distort CMB E-polarized photons into a lensed B spectrum which has been repeatedly recorded [14][15], the cosmological B-mode signature remains undetected; its pursuit is one of the key focuses of cosmology today. While the well-measured E-mode spectrum as it correlates with temperature is generated largely by scalar perturbations in the early universe and so contains information about the formation of large structures, B-mode generation via primordial gravitational waves is predicted by models of cosmological inflation. A detection of the cosmological B-mode signal would therefore be strong evidence for such a model, and would constrain r, the ratio of the power in the tensor and scalar perturbation modes generated by these gravitational waves, indicating the energy scale on which the period of inflation occurred. Fig. 1.1 depicts B-mode spectra for a range of these energy scales.

1.3 Detection

Faced with such a valuable prize, multiple experiments are underway, attempting to either resolve the inflationary B-mode polarization, or to tighten the constraints on its scale. For instance, the best limit to date on the tensor to scalar ratio is provided by the *Planck* collaboration in conjunction with data from BICEP2 and the Keck Array: $r < 0.064$ at a 95% confidence level[16]. Further lowering this number (or eventually making a detection of the primordial B mode itself) relies on ever-improving instrument capabilities – particularly, on the diminuation of the noise contribution of the instrument and in the number of repeated measurements it can provide in a given amount of time.

1.4 Noise

To observe a signal, it must be separable from astrophysical foregrounds, as well as visible above the noise and systemic contamination of the instrument and its environment. In the relevant case of observing the CMB, this signal is a photon emitted more than 13 billion years ago at the surface of last scattering. In some environments, such as for a space-based observer looking through a perfectly cold lens at an otherwise empty universe, these photons might be the only signal available. But in more practical terms, they are some of many, and distinguishing them from photons originating from other sources is key.

For the ground-based observer, the primary source of energy deposited on an instrument is Earth's atmosphere. The second source will be from the instrument itself: the materials in the instrument's mirrors or lenses will have some temperature (typically a temperature much greater than the 4K CMB), and will emit light accordingly. Then, finally, is the contribution from the CMB photons themselves. Naturally it is desirable to minimize these first two contributions in order to isolate the third. This may be accomplished by sensible choices of environment, for example constructing the instrument in a place with low amounts of atmospheric humidity to reduce absorption, or an area with low atmospheric turbulence to reduce the effects of varying densities and indices of refraction, or simply some place with less atmosphere overall such as (ideally) space or (more practically) a high altitude. The contributions from the optics themselves are somewhat less avoidable, but can be optimized by choosing materials with low emissivity in the observation band, and by reducing their temperature.

Keeping the detectors themselves cold also minimizes their own noise contribution. Any resistive part of a detector will produce thermal Johnson noise with a spectral density as a function of its resistance, R, and temperature, T, of $4k_BTR$ (where k_B is the Boltzmann constant), and even at thermal equilibrium, random thermal (phonon) exchange between the detector and its surrounding heat bath will result in a temperature fluctuation with spectral density $4k_BT^2g\gamma$, where g is the thermal conductance of the link to the bath, and γ is a coefficient accounting for thermal gradients along the link.

After minimizing unwanted contributions from the instrument, its environment, and from the inherent noise produced by its detectors, the next step in improving the sensitivity of an instrument lies in its electronics. Most if not all modern telescopes employ electronic detection mechanisms of varying degrees of complexity. These systems handle all aspects of the signal detection chain: from the initial interaction with an incident photon, to the transportation of the signal to the first amplification stages, out to its final isolated and processed state. At each point, these electronics contribute noise to the signal: from random electron motion in conductors (as in the detectors), the characteristic input voltage and current noise of amplifiers, all the way up to the errors introduced by quantization during digitization. While the third is beyond the scope of this work, the handling of the first two sources of noise will be treated in some detail.

While it is not possible to create a system which contributes no noise, it is possible to create one in which its noise contribution is insignificant compared to one which cannot be reduced. Detecting photons is a stochastic process wherein the arrival time of the photons at the detector is not uniform, and (ignoring the effects of photon correlation) the noise-equivalent power (NEP) this irregularity produces is a function of the optical power P_{opt} deposited on each detector: $\sqrt{2P_{opt}h\nu}$[13]. This sets an absolute lower bound on the noise power that can be produced in an instrument, to which all other noise sources should be subdominant. See Table 1.1 for an overview of noise sources in an example multiplexed readout system.

1.5 Repeated measurement

Another opportunity for improvement in the performance of an instrument is to increase the number of measurements that it can make simultaneously. The improvement here comes from an overall measurement uncertainty that decreases as $1/\sqrt{N}$ as the number of measurements, N, increases.

Example system parameters with $T = 0.55K$, $\gamma = 0.5$, $g = 165pW/K$, $P_{opt} = 11pW$, $V_{bias} = 3.2\mu V_{RMS}$ [17]			
Noise source	Equation (NEP)	Example system NEP (aW/$\sqrt{\text{Hz}}$)	Example system NEI (pA/$\sqrt{\text{Hz}}$)
Bolometer (Johnson)	$\sqrt{4k_B T P_{elec}}/\mathcal{L}$	$21/\mathcal{L}$	$9/\mathcal{L}$
Bolometer (phonon)	$\sqrt{4k_B T^2 g\gamma}$	37	16
photon	$\sqrt{2P_{opt}h\nu}$	47	21
readout	$\sqrt{\Sigma i_n^2}\frac{V_{bias}}{\sqrt{2}}$, for all sources i_n in the readout system	$< NEP_{photon}$	

Table 1.1: Summary of noise sources for an example fMUX readout architecture operating TES bolometers with an incident optical power, P_{opt}, and operated at bias voltage, V_{bias}[17]. The sources are computed as a noise equivalent power (NEP), and as a noise equivalent current (NEI) through an example bolometer. Bolometer temperature is represented by T, frequency by ν, Planck's constant by h, and the Boltzmann constant by k_B, with the factor of $1/\mathcal{L}$ approximating the suppression of the bolometer Johnson noise by the loop gain of the system.

This may be done simply by measuring more times – that is, making the same measurement repeatedly for some duration. In our fast-paced modern world, many experimenters may find this unsuitable; an alternative is to build many separate experimental setups and operate them all simultaneously. In a telescope looking to measure photons from the CMB, this entails building an instrument with a high number of detectors (bolometers). Each bolometer sees a patch of sky distinct from its neighbours, and the dominant source of measurement uncertainty for each (the random arrival time of incident photons) is unrelated to that of the others. Each bolometer's signal may therefore be considered an independent measurement. State-of-the-art CMB experiments on the sky today have many thousands of detectors.

However, this apparently simple solution presents some practical challenges. A signal must be transported – or, *read out* – from each of these N independent devices to a stage at which it can be interpreted by the experimenter. This involves some sort of contact with the bolometer, typically through a wire. As a prior part of the optimization of this system involved minimizing the temperature of the system, these bolometers are typically kept at sub-kelvin temperatures. Connecting thousands of wires, even just one to each individual detector, would conduct not only the signal, but also a catastrophic amount of heat from the room-temperature electronics. A more efficient readout scheme is required.

1.6 Multiplexing

To avoid a one-to-one scaling relation between the number of detectors in an instrument and the number of wires connecting to them, some sort of multiplexing scheme is required. In general, multiplexing involves the transportation of multiple signals down a single path, and can be accomplished through several strategies, including microwave multiplexing, frequency-domain multiplexing, and time-domain multiplexing (for a discussion of each these strategies as used by recent on-sky experiments, see, for example, [19], [17], and

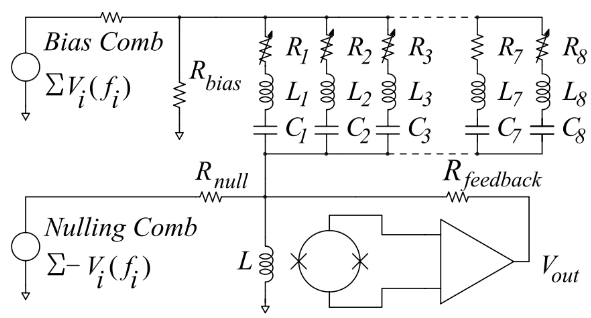

Figure 1.2: A schematic of an frequency-multiplexed readout system, with eight LCR_{bolo} readout channels, a superconducting quantum interference device (SQUID) amplifier, and nuller implementation (see 2.2).[18]

[20], respectively). The last of these strategies is perhaps the most intuitive, in which a group of detectors takes turns transmitting their signals along a wire – spacing themselves out in time. Alternatively, the detectors can be spaced out in frequency: frequency-domain multiplexing (fMUX). In this architecture, detectors are read out simultaneously along a single wire, with their signal information modulating an applied sinusoidal bias. This efficient architecture has so far been demonstrated to be able to read out up to 128 bolometers.[21]

Frequency-multiplexed schemes are in use in some of the world's most advanced millimeter-wavelength telescopes, operating up to the current world record of 16,140 bolometers at the South Pole Telescope, where these remarkable numbers combine with arcminute resolution and photon-noise-limited readout systems to allow microkelvin measurements of the CMB[22][23].

The handling of these signals at room temperature requires at least one stage of amplification. In all existing systems, the first stage of this is accomplished using superconducting quantum interference device (SQUID) amplifiers, which, while technically well-suited to this purpose due to their low noise and input impedance, present operational challenges particularly when scaling to higher numbers of detectors. The design and characterization of a prototype alternative readout amplification scheme for fMUX architectures which does not rely on SQUIDs is the focus of this work.

Chapter 2

Motivation

Millimeter-wavelength cosmology is a mature field, with many notable scientific contributions, instruments attaining photon-noise-limited performance, and innovations continuing to push the bounds of what is observable. It may therefore appear that there is little motivation for improvement in terms of detector readout technology. However, as readout systems and detectors themselves are already operating at the physical limits of their performance, the path towards making deeper measurements of the CMB in the near-term lies in increasing the number of existing detectors themselves. In this chapter, the case is made for investigating new readout technologies which might facilitate this move to higher detector counts, including motivating factors in existing and future readout systems, such as high multiplexing factors (the number of detectors which may be operated by a single readout module) and the choice of amplification scheme.

2.1 Multiplexing factors

As discussed in the prevous chapter, an increase in detector numbers corresponds to an increase in the thermal costs on an experiment. This cost can be strongly mitigated by multiplexing, but there are constraints on the number of detectors which can be effectively operated by a single readout module, as well as difficulties in increasing the number of modules themselves.

In fMUX architectures, individual bolometers must be kept sufficiently separate in frequency space so as to minimize signal sharing (crosstalk) amongst neighbours. A natural solution to allow additional bolometers on a single readout channel would be to simply increase the total bandwidth of the readout module to add space for new detectors. However, practical constraints on the operation and design of the amplifier through which all these bolometer signals must pass restrict a single module's allowable bandwidth. Additionally, the amplifiers favoured in fMUX systems are superconducting quantum interference devices (SQUIDs), which, while highly effective for this use, present some operational difficulties when scaling an experiment to larger detector counts.

2.2 SQUIDs

Superconducting quantum interference devices (SQUIDs) are frequently used as cryogenic, very low noise, low input impedance, transimpedance amplifiers. A superconducting loop broken by two insulating (Josephson) junctions (Figure 2.1), fed by a nearby inductive coil, a SQUID, however, is a far cry from a traditional amplifier. Current through the input coil drives a magnetic field, of whose flux a portion passes through the loop, and in response to which the SQUID creates a voltage. While the details of the operating principles of SQUIDs are beyond the scope of this thesis (see [24]), their use and application in millimeter-wavelength cosmological experiments are the main motivation for the work described herein.

SQUIDs are widely used in mm-wavelength experiments, and with good reason. Their combination of low input impedance (for example, from 0.5 to 2.3Ω as operated in an existing system, over frequencies from 1.5 to 6MHz [22])) and low input noise (typically $< 4\text{pA}/\sqrt{\text{Hz}}$ [17]) allow them to be effective first-stage amplifiers in operation with transition-edge sensor (TES) bolometers, the dominant detector technology in the field, which are stable power-measuring devices only when coupled to a low input impedance readout device. However, they present certain operational challenges.

The first of these challenges is inherent to their physical properties. A SQUID is an extremely sensitive magnetic field detector, and therefore must not only be kept thoroughly shielded from any contaminating environmental

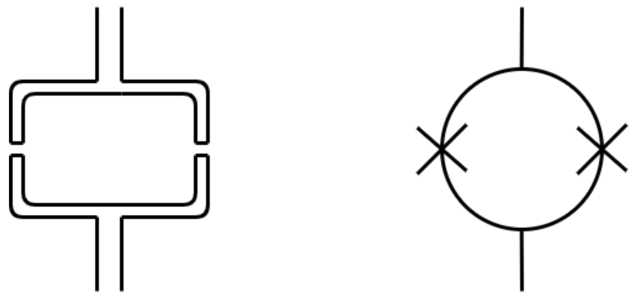

Figure 2.1: A schematic *(left)* and circuit symbol *(right)* for a superconducting quantum interference device (SQUID). A loop of superconducting wire, broken by two Josephson junctions, creates a voltage in response to an applied magnetic field, generated by current flowing through a nearby inductor (not pictured).

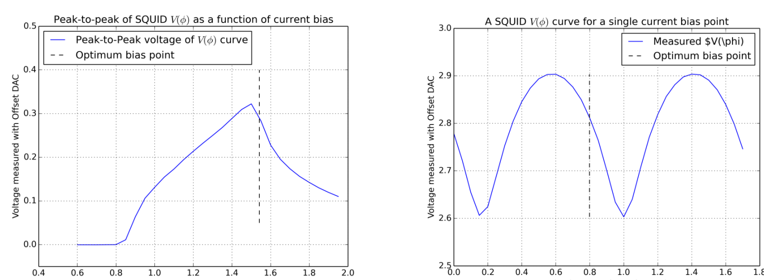

(a) (b)

Figure 2.2: Tuning response of a SQUID while determining optimum biasing parameters *(dotted lines)*. *(a)*: voltage per applied magnetic flux ($V(\phi)$) as a function of applied current bias. *(b)* $V(\phi)$ response to applied voltage bias.[25]

fields, but also provided with a magnetic flux bias, supplied by sending a DC biasing current down the adjacent inductive input coil (see Figure 1.2). A second biasing signal is required to set a baseline current across the SQUID itself[25]. The levels of these two biases depend on the state of the SQUID, which is determined by the magnetic flux passing through it as it cools to a superconducting state, and their optimized configuration cannot be determined prior to cooling. This optimization (see Figure 2.2) must therefore be performed on each individual amplifier, each time it is cooled to operational temperature. This represents experimental downtime, as bolometers cannot be operated until this process is complete.

A SQUID's linear operating regime presents a further challenge. The range of applied magnetic flux values to which a SQUID will have a linear output voltage response is very narrow. It is therefore difficult not to allow too much signal through the SQUID, resulting in an nonlinear result – not a desirable quality for an amplifier, particularly as experiments look to increase the number of multiplexed detectors (and thereby the scale of the signal) per SQUID channel. This issue can be mitigated by invoking an active nulling scheme, such as employed at the South Pole Telescope, which digitizes the output of the SQUID, synthesizes an inverted copy of the current headed to the SQUID and feeds it back into the input coil. This results in the SQUID seeing near zero input current, allowing it to continue linear operation. However, such a system is not only complex, but requires running additional connections from cryogenic stages to room temperature and back again, and introduces an additional source of noise from the digitization and synthesis of the nulling signal.[25]

2.3 Case for an alternative system

Generally speaking, an ideal readout system might be designed to have the following characteristics:

- Photon-noise-limited performance. A readout system should contribute as little noise as possible, and strive to be limited in that respect by the lower bound set by noise contributions from the incident light itself; for an example system such as the one described in Table 1.1, this noise contribution should be $\lesssim 21$ pA/$\sqrt{\text{Hz}}$

- High gain. Signals generated by detectors must be sufficiently amplified so as to be discernable above the noise of room temperature electronics; e.g. the ratio of the system's output voltage to its input current, its transimpedance, should be > 200.

- Low thermal loads. The number of connections between hot and cold stages in an instrument should be minimized, to allow effecient cryogenic operation; to keep total thermal loading from all readout wires $<< 1\mu$W.

- On-sky efficiency. A system should minimize its necessary downtime and spend as much time as possible observing, seeking to improve upon the 25 - 60% uptime of existing experiments (see, for example, [26]).

– Scalability. As new experiments are designed with larger numbers of detectors, a readout system should adapt to this increased payload, scaling linearly in cost and thermal load, without incurring additional architectural complexity.

Present fMUX architectures using SQUID amplifiers attain the first two handily, but improvements may be made upon the latter three by changing to a different amplification scheme, one with a larger dynamic range and without the need for individual tuning parameters. The most readily attainable gains in the design of a readout system are therefore to be made not in improving its noise or sensitivity performance, but rather in reducing its complexity, improving its on-sky efficiency, and making it more easily scalable to large numbers of detectors.

Chapter 3

Transformer-Coupled System

While it is worthwhile to look to improve upon the adaptability, complexity, and efficiency of existing systems, this should not be done at a cost to their performance. In designing an alternative system, the standards of noise contribution and signal gain set by existing state-of-the-art systems must be met, if not also improved upon. This section details the design of an alternative fMUX readout architecture, which replaces the SQUID with a transformer-coupled field-effect transistor (FET) amplifier, in a novel low-impedance configuration. The use of these simple components dramatically increases the linear operating range of the system, reduces the thermal load on sub-kelvin cryogenic stages by not requiring wiring for complex nulling arrangements, and altogether removes the need to spend time tuning the SQUID operating points. The system is developed as a proof of concept, and makes use of existing fMUX technology wherever possible.

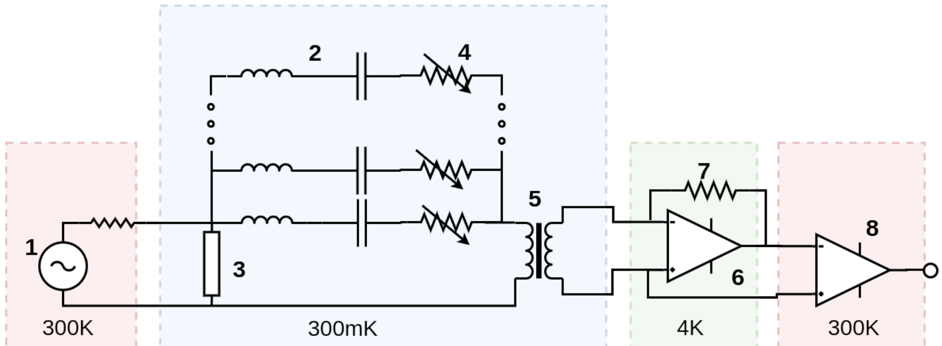

Figure 3.1: Schematic diagram of the proposed alternative readout system, featuring a transformer-coupled field-effect transistor transimpedance amplifier *(5-7)* in a frequency-multiplexed architecture *(1-4)*, with warm secondary amplification *(8)*.

3.1 Filters and biases

As in existing fMUX architectures, multiple detectors are to be read out simultaneously through operation at separate frequencies. This involves applying a sinusoidal bias voltage to each detector, widely spaced in frequency over some bandwidth. These bias signals are generated by an array of synthesizers within a digital signal processing platform [27] *(1 in Figure 3.1)* and transmitted as currents to the bolometers over a single wire pair, where their voltage across the detectors is set by a biasing impedance, typically a resistor *(3)*. One tone is generated per detector, and an inductive-capacitive (LC) filter network *(2)* separates each from its neighbours, ensuring that it sees primarily its own bias frequency. This filter bank is composed of superconducting niobium traces forming a network of 68 parallel LC resonators, with an identical set of spiral inductors across all channels defining the bandwidth of each, and the resonant frequency of each channel set by the interdigitated capacitor and spaced logarithmically over 6MHz [22]. As the network is superconducting at operational temperatures, the resistance of each channel in the filter is zero, the quality (Q) factor of the resonator is ultra-high, and the resulting peak is extremely narrow (on the order of a few hundred Hz), providing effective isolation from neighbouring bias frequencies.

3.2 Detectors

The detectors typically operated by fMUX readout schemes are transition-edge sensor (TES) bolometers. These are small strips of metal, held at a temperature on the threshold of their transition between normal resistance and superconductivity, and coupled to an antenna. Incoming optical power deposits a small amount of thermal energy on the film, modulating the current that flows through it by attempting to push it out of its superconducting transition. Keeping the sensors in transition through negative electrothermal feedback allows attowatt-scale sensitivity to sky signals. (see [13] for a more in-depth discussion).

However, for the purposes of developing and characterizing this alternative readout system, such a sensitive instrument is not required – in fact, light sensitivity is superfluous to the initial prototyping stages, and so these TES bolometers are replaced with 1- and 2 Ω resistors *(4)* while the system is in development (these resistors, along with the multiplexing filter comb,

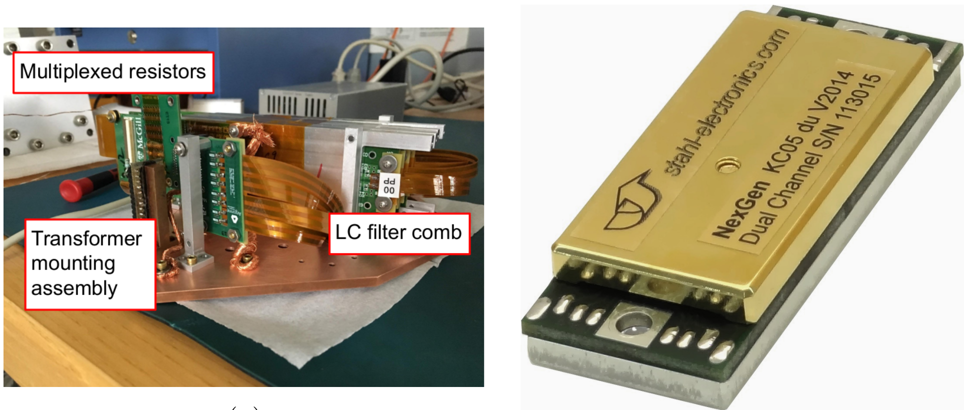

(a)

(b)

Figure 3.2: *(a):* multiplexing hardware (filter comb inside aluminum shield, resistors in place of bolometers during testing) and transformer mount on the desktop. This assembly is then installed inside the cryostat on the 300mK stage. *(b):* close-up of the GaAs FET assembly, the KC05d from Stahl Electronics[28]. It is 5.45cm in length, and is mounted on the 4K stage of the cryostat.

are shown assembled on the desktop in Figure 3.2a). These are chosen to be comparable to the normal resitance of the TES sensors in use with on-sky fMUX architectures. As their resistance is constant over the range of operational cryogenic temperatures (< 4K), they provide a simple stand-in to characterize the rest of the readout system. Conveniently, like a bolometer, they also produce a signal that the system can measure - the variation in their thermal Johnson noise as a function of temperature.

3.3 Transformer-coupled amplifier

The ability to capture CMB photons is not useful without the ability to eventually interpret the information they convey at room temperature. To arrive at this stage, the detection signal must first be amplified; signals from bolometers operated at sub-kelvin superconducting transition temperatures are extremely small. They can only be handled at their initial scale in these cryogenic regimes because the superconducting elements that they interact with do not degrade or overwhelm them with thermal noise. To preserve a high signal-to-noise ratio as they are transported to warmer stages of the experiment, however, some process of amplification is needed. This amplification must contribute very little noise, as the signals it handles are still very small, and also have a high gain to increase the signal magnitude to a useable scale: greater than the input voltage noise of the warm electronics.

In this proposed readout system, the first stage of this amplification is a transformer-coupled amplifier. The amplifier *(6)* used in the prototype system is the KC05d, a gallium-arsenide field-effect transistor (GaAs FET), designed and manufactured commercially by Stahl Electronics [28]. The KC05d, pictured in Figure 3.2b, operates cryogenically at 4K with an open-loop gain of $A_0 = 20$, and is chosen for this use for its extremely low input voltage and current noise contributions ($0.33\mathrm{nV}/\sqrt{\mathrm{Hz}}$ and $17\mathrm{fA}/\sqrt{\mathrm{Hz}}$, respectively). FET amplifiers are characteristically high-impedance (the KC05d, for instance, has an input impedance of $> 40\mathrm{M}\Omega$), making them typically poorly-suited for use with 1Ω TES bolometers, which operate as current-modulating devices and are unstable unless coupled to an input impedance much smaller than their own. To overcome this, the amplifier is run as a transimpedance amplifier in an inverting negative feedback configuration *(7)*, in which a feedback resistor connects the amplifier's output to its inverting (negative) input. This sets its input impedance to be

$$Z_{in,amp} = \frac{R_f}{A_0 + 1} \simeq \frac{R_f}{A_0} \tag{3.1}$$

and its transimpedance (the ratio of its voltage output to its current input) to be

$$Z_{trans,amp} = \frac{R_f}{A_0^{-1} + 1} \simeq R_f \tag{3.2}$$

(see Appendix A for more detail on the origin of these relations). However, the input impedance still cannot be made arbitrarily small, as diminishing choices of R_f result in diminishing returns on transimpedance, a necessary part of the system's amplification stage. For instance, the best low-noise amplifiers which might be used as the front end of the system's warm electronics typically contribute $1\mathrm{nV}/\sqrt{\mathrm{Hz}}$ [17]; the transimpedance of the cold system must transform the miniscule signal current to at least this voltage level.

Further reduction in the input impedance of the FET is accomplished by coupling its input to a high-turns-ratio transformer*(5)*. With the detectors and LC comb network in series with its primary coil, the transformer lowers the impedance of the FET as seen by the detectors by a factor of the square of its turns ratio, N (the input impedance of a transformer is given by R_L/N^2, where R_L is the load impedance (i.e., the impedance present at the secondary coil), rather than $2\pi f L_p$ as would be expected if considering the primary coil, L_p, to be a simple inductor; see Appendix C for more detail). The coupled system therefore has an input impedance of

$$Z_{in} = \frac{R_f}{N^2(A_0 + 1)}, \tag{3.3}$$

and a transimpedance of

$$Z_{trans} = \frac{R_f}{N(A_0^{-1} + 1)} \simeq \frac{R_f}{N}. \tag{3.4}$$

The stray inductance of connections to and from the detectors and filter comb compromises detector stability in fMUX systems, such that special low-inductance striplines are required for operation. In the prototype system, the transformer is kept adjacent to the comb on the sub-kelvin stage to minimize these strays at its input, and acts to step down the inductance of the connections from its output to the amplifier. This allows these connections to be simple wires of arbitrary length.

3.4 Optimization

For an amplifier with fixed current noise, voltage noise, and gain ($v_{n,FET}$, $i_{n,FET}$, and A_0, respectively), the main parameters in the system are the transformer's turns ratio, N, and the value of the feedback resistor, R_f. The system's input impedance, Z_{in}, must be low ($<< 1\Omega$) in order to maintain the stability of TES detectors. Optimization of this system revolves around minimizing the current noise at the detectors – that is, the total noise of the readout system, referred to the transformer primary loop as a current, i_n – while keeping the system's input impedance low.

This total current noise is the quadratic sum of several individual noise currents from various uncorrelated sources in the system. The relevant quantities (derived in Appendix A) are as follows, referred to the transformer primary:

– The input voltage noise of the KC05d FET, $v_{n,FET}$:

$$i_{n,FET,v_n} = v_{n,FET} \frac{R_f}{R_{bolo} N^2} \frac{1}{Z_{trans}} = v_{n,FET} \frac{A_0^{-1} + 1}{R_{bolo} N} \tag{3.5}$$

– The input current noise of the KC05d FET, $i_{n,FET}$:

$$i_{n,FET,i_n} = i_{n,FET} \frac{R_f}{A_0^{-1} + 1} \frac{1}{Z_{trans}} = i_{n,FET} N \tag{3.6}$$

– Johnson noise from the feedback resistor:

$$i_{n,R_f} = \frac{\sqrt{4k_BTR_f}}{Z_{trans}} = \sqrt{\frac{4k_BT}{R_f}}N(A_0^{-1}+1) \tag{3.7}$$

– The input voltage noise of secondary amplification stages:

$$i_{n,aux,v_n} = \frac{v_{n,aux}}{Z_{trans}} = v_{n,aux}\frac{N(A_0^{-1}+1)}{R_f} \tag{3.8}$$

These quantities, as a function of the value of R_f for a given Z_{in}, are shown in Figure 3.3a). Adding these in quadrature gives the relation:

$$i_n^2 = \left(v_{n,FET}\frac{A_0^{-1}+1}{R_{bolo}N}\right)^2 + (i_{n,FET}N)^2 + \left(\sqrt{\frac{4k_BT}{R_f}}N(A_0^{-1}+1)\right)^2 + \left(v_{n,aux}\frac{N(A_0^{-1}+1)}{R_f}\right)^2 \tag{3.9}$$

A constraint may be added by choosing the input impedance of the system; ideally, $Z_{in} << 1$. This allows expressing the turns ratio N in terms of R_f as:

$$N = \sqrt{\frac{R_f}{Z_{in}(A_0+1)}} \tag{3.10}$$

This relation is shown in Figure 3.3b. The total noise in the system now depends solely on the value of the feedback resistor, as shown in Figure 3.3a. Its value may then be chosen as close to the minimum of the total input-referred noise current as practicality in input impedance and turns ratio allow.

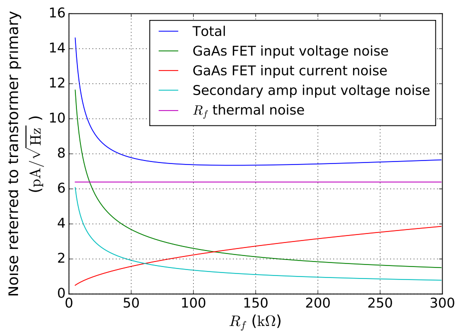

(a)

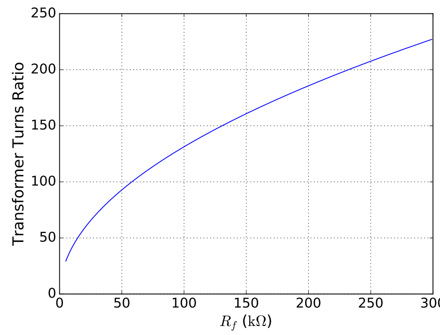

(b)

Figure 3.3: *(a):* System input-referred current noise as a function of the amplifier feedback resistance, R_f, with the transformer turns ratio, N, chosen at each point such that the system input impedance, Z_{in}, is fixed at 0.2Ω. The relation of N to R_f for a fixed Z_{in} is shown in *(b)*. These plots are used to choose R_f to minimize the total noise in the system. Practicality in fabrication is also considered when selecting a feedback resistance, so as to not require a transformer with too extreme a turns ratio (values of $N >> 50$ for transformers in this context pose a challenge for construction; see 4.2). For nearly all values of R_f, its thermal Johnson noise dominates the noise of the readout system, and its contribution is fixed for a given temperature, system input impedance, and amplifier open-loop gain.

Chapter 4

Design and Construction

In this chapter, practical design considerations for a transformer-coupled fMUX system are discussed, including biasing, the intricacies of transformer construction, and alternative feedback topologies.

4.1 Biasing

In an fMUX system, detectors are operated at individual bias frequencies, which are generated as currents by a room-temperature digital synthesis platform [27]. This is transformed into a voltage across each detector by a bias impedance in parallel with the channels.

In the prototype transformer-coupled system, this biasing impedance is chosen to be a resistor (50mΩ), in keeping with established fMUX architectures [17]. While a resistor minimizes complexity with its frequency-

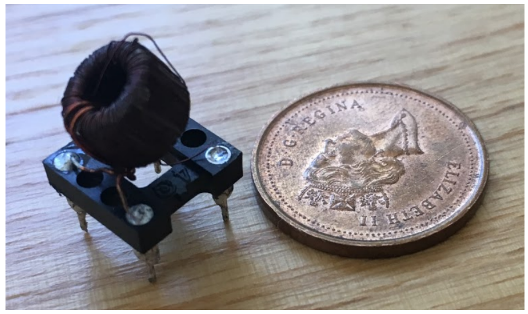

Figure 4.1: The transformer used in the prototype circuit. A molypermalloy powder core wound with copper wire, it has a turns ratio of $N = 100/2 = 50$, and was custom-built at McGill University for this purpose [29].

independent response, it is dissipative and therefore is a source of thermal loading, particularly when kept on the coldest cryogenic stage, which is generally the least powerful. Additionally, it produces a Johnson noise current (though in this configuration, this current is $< 1\text{pA}/\sqrt{\text{Hz}}$, small enough to be negligible). These may both be mitigated by instead choosing to set the detector bias voltage with a capacitive or inductive divider, as in [21].

4.2 Transformer

The prototype is designed to use existing technology wherever possible, to both maximize compatibility and minimize construction costs and labour. Therefore, it utilizes a 68-channel niobium-trace LC filter comb of the type employed on the South Pole Telescope and a commercially-available GaAs FET amplifier from Stahl Electronics [28], with the only newly-constructed component being a custom-built transformer.

The transformer used in the prototype circuit was designed and hand-wound in the McGill lab specifically for this purpose [29]. It utilizes a compact molypermalloy powder (MPP) core (Arnold Magnetics MP-018125-8), wound with copper wire.

The ability to operate at both cryogenic temperature and MHz frequency are rarely found together in the same core material [30]. Molypermalloy is a nickel-iron-molybdenum alloy, which combines low core losses with a wide range of magnetic permeabilities, μ, which are preserved into the MHz range [31], making this a good candidate material for this application. To verify that these qualities are preserved down to cryogenic temperatures, several transformer cores were wound as simple inductors and mounted inside a cryostat, and their complex impedances measured over the course of a cooling run (down to 4K). It was found that for the type of core used (MPP with nominal $\mu = 125$), the decrease in permeability at low frequency (1MHz) from 300 K to 4 K was 9%. At high frequency (10MHz), this change was measured to be 15%. These effects were even smaller for a lower μ MPP core ($\mu = 60$), where the changes were $< 5\%$ for all frequencies tested.[1]

It has two windings on its primary coil and 100 on its secondary, for a turns ratio, N, of 50, and primary and secondary inductances of $L_p = 280$nH and $L_s = 672\mu$H, respectively. Copper is used for wires on both the primary and secondary coils, as the short length and large gauge of the primary coil results in negligible impedance (R_p in Figure 4.2 is < 1mΩ), and any

[1] E. Egan, personal communication, McGill University, 2019.

impedance of the longer, smaller-gauge secondary is diminished by a factor of N^2 when reflected to the primary loop (R_s in Fig. 4.2; this is measured to be 3Ω at the secondary, or 1.2mΩ at the primary). Additionally, using a normal conductor (instead of, for example, superconducting niobium wire) allows the transformer to operate at temperatures beyond most transition temperatures, facilitating testing (see 5.2.2).

Though striving for the optimized parameters described in 3.4, the value of N was also impacted by manufacturing constraints: there is a physical upper limit on the number of wraps which may be placed on a small core (the prototype utilizes a core with a 6.9mm outer diameter, chosen to be comparable to the footprint of a typical SQUID amplifier in existing fMUX systems), and practicality in handling limits the lower bound of the wire gauge. While large increases in N might still be affected by small decreases in the primary wrap count, to effectively operate a transformer, the impedance of the primary coil inductor must be larger than the transformer's primary-referred load by a factor larger than 1 (in this system, chosen to be larger by a factor of 5 so as to keep low-frequency losses below 20%; this reasoning is explained in more detail in Appendix C). The inductance of the coil is given by $A_L N^2$, where A_L is a function of the core's magnetic permeability, μ, and its physical geometry. The core used in the prototype has $\mu = 125$ and $A_L = 70\text{nH/turn}^2$. Selecting the minimum operating frequency of the system to be 1MHz and having determined the primary-referred input impedance of the FET amplifier in current follower mode to be $\sim 0.2\Omega$, the minimum

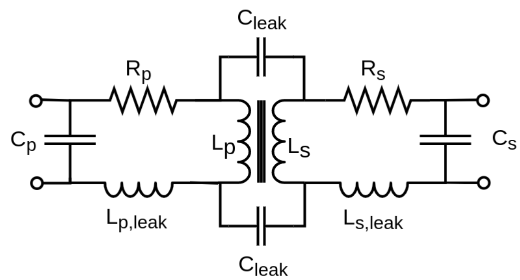

Figure 4.2: Model of a transformer with relevant strays, as characterized in [29]. The primary and secondary inductances, L_p and L_s, the principal inductors of the transformer, are created by the winding of wire around the transformer core. The other components shown are stray properties of these windings: C_p and C_s are capacitances between the turns within a coil, R_p and R_s are the resistances of the coil wires, $L_{p,leak}$ and $L_{s,leak}$ are leakage inductances created by an imperfect magnetic coupling across the transformer, and the two C_{leak} are leakage capacitances from one coil to another.

primary coil inductance is $\frac{1\Omega}{2\pi 1\text{MHz}} = 160\text{nH}$, thereby requiring at least two turns (refer to Appendix C for more detail).

4.3 Considerations

Beyond the turns ratio dictated by the parameters of the prototype system, a key performance characteristic for the transformer is the magnetic coupling between its primary and secondary coil. Commonly denoted by the coupling coefficient, k, this is a function of the geometry of the core and windings, and is a measure of the fraction of the magnetic flux lines generated by one coil which pass through the second. A perfect coupling (all flux lines passing through the second winding; $k = 1$) is sought for this system, as any uncoupled fraction of the magnetic field leads to stray inductance, which acts as an impedance in series with the transformer ($L_{p,leak}$ and $L_{s,leak}$ in Figure 4.2). This increases the system's input impedance, especially at higher frequencies, diminishing its ability to effectively operate current-sensing TES bolometers. The leakage inductance of each coil of the transformer may be determined by measuring its inductance at frequency f as $L^{\sigma} = {}^{Z}/_{(2\pi f)}$ while a short is set across the opposite coil. The coupling coefficent may then be calculated as $k = \sqrt{1 - {}^{L^{\sigma}}/_{L}}$, where the coil inductance, L, is obtained similarly, but with the opposing coil left open (see [32] and [33]).

Several transformer designs were tested. The cores were chosen to have a compact geometry, allowing installation in existing infrastructure, where a typical SQUID footprint is $\sim 1\text{cm}^2$. Winding was therefore done with thin copper wire, and many cores were wound and characterized to maximize both the turns ratio and the coupling.

The highest coupling was achieved when winding a single layer of turns on the secondary coil (Figure 4.3a), but this places a strong limit on the number of windings that can be placed onto the core based on its size. Finer wires were also tested, but were found to be prone to snarls and breakage, particularly when working on such a small object, making achieving high wrap counts unfeasible. Using a more manageable wire gauge and making a second layer of windings (Figure 4.3b) produces acceptable coupling, but must be done carefully to avoid capacitance between turns (C_s and C_p in Fig. 4.2), which reduces the effective N by providing a short across the

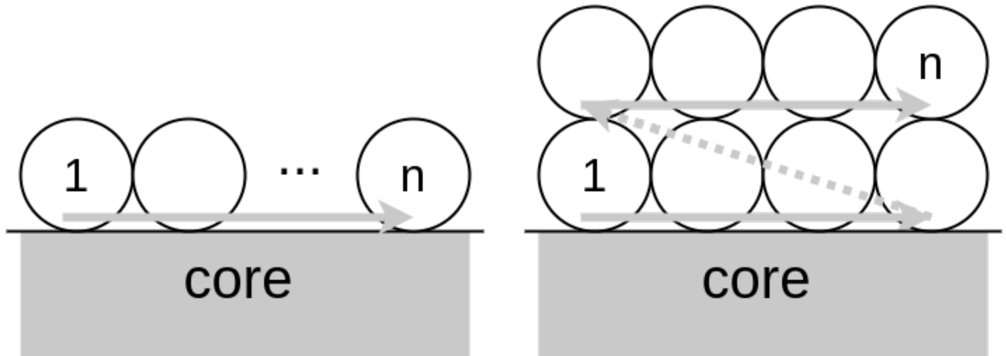

(a) (b)

Figure 4.3: Two transformer winding strategies, shown in cross-section with arrows indicating the direction in which the windings are applied. In *(a)*, a single layer is used, placing turns side by side until the desired number, n, is reached. This strategy is simple and achieves good coupling and intra-winding capacitance, but strongly limits the number of turns that can be applied on a small core. In *(b)*, after a number (e.g. 20) of turns is placed on the core, the winder returns the wire to the beginning of the section and begins a new layer of the same number atop the first. These sections are repeated around the core until the desired number of turns is reached. This strategy is economic in terms of space on the core, but care must be taken to ensure that the number of turns separating neighbouring wires (particularly, between layers) is not large, in order to avoid intra-winding capacitance.

coils at high frequency; this is primarily a concern on the secondary coil, as $C_s >> C_p$ due to the difference in turn count. An additional concern when crowding high turn counts onto small cores is that allowing the primary and secondary coils to overlap for a significant length of wire may allow current to bypass the transformer at high frequencies by capacitive coupling (C_{leak} in Figure 4.2), although in the cores tested, the effect of this was found to be negligible [29]. A strategy of winding < 20 adjacent turns on the bottom layer, returning directly to the start point, and winding a second layer atop

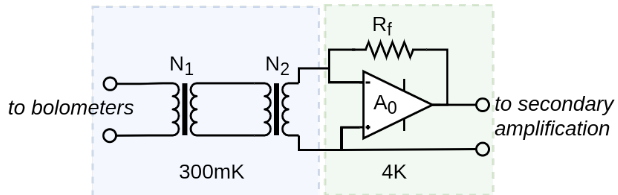

Figure 4.4: An alternative design for the transformer-coupled system. Here, two cascaded transformers couple the FET amplifier to the bolometers. The first utilizes a bifilar winding strategy with a low turns ratio, N_1, while the second is singularly wound and has a higher turns ratio, N_2. The near perfect coupling achieved by most bifilar transformers allows the impedance of the second transformer's leakage inductance to be reflected to the first primary, diminished by a factor of N_1^2, minimizing its impact on the system.

the first, was found to be effective in preserving N and resulted in useable coupling. However, the overall determination was that achieving couplings much greater than $k \sim 0.85$ for $N \gtrsim 50$ was not feasible on such small cores (see Appendix B).

The impact of stray inductance due to poor coupling may be mitigated by clever topology. An alternative design not implemented for the prototype might feature two cascaded transformers, as shown in Figure 4.4, instead of the singular scheme used here. In this design, two transformers are constructed: the first with a very high coupling coefficient and low turns ratio, $N_1 < 10$, and the second with a higher turns ratio, $N_2 \sim 50$. The high coupling on the first transformer may be achieved using bifilar winding, a style in which the primary and secondary wires are wound together around the core; an MPP core of the same type as those described above, with a bifilar turns ratio of 10:10, was measured in the McGill lab to have a coupling coefficient of $k = 0.99$ [2]). Alternatively, simply using a high number of turns on the primary—facilitated by having N_1 be small—similar values of k can be achieved. With such high coupling, the first transformer will create little leakage inductance. What stray impedance is generated by the second transformer is reflected to the primary of the first, diminished by a factor of N_1^2, and the total turns ratio of the cascaded system is $N_1 N_2$. While this design was not tested for the prototype described in this thesis, it may be promising for low input impedance and high N, and may be a worthwhile avenue for future work.

4.4 Feedback

The GaAs FET in the prototype circuit is operated as a transimpedance amplifier, with feedback connecting the FET's output to its inverting input at the transformer secondary coil. This sets the transimpedance of the cold stages of the system to be $\frac{R_f}{N(A_0^{-1}+1)}$, and input impedance to be $\frac{R_f}{N^2(A_0+1)}$, with N the transformer turns ratio, R_f the value of the feedback resistor, and A_0 the FET open-loop gain (see Appendix A). R_f is clearly of high importance as a parameter of the system, as it must be chosen to strike an optimized balance between high gain and low input impedance (see 3.4). Two alternate configurations were investigated during the design of the prototype transformer-coupled system, in which practical optimization concerns were

[2] E. Egan, personal communication, McGill University, 2019.

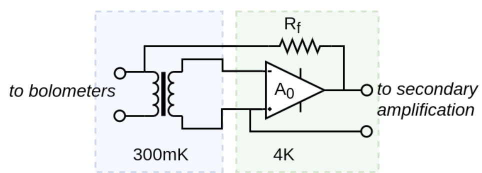

(a)

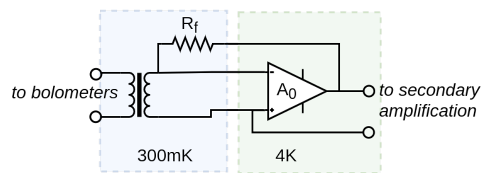

(b)

Figure 4.5: Alternative amplifier feedback configurations investigated during the development of the main prototype. *(a):* feedback connecting the output of the amplifier to the transformer primary coil. This creates a virtual ground at the transformer input, shorting out stray inductance caused by imperfect magnetic coupling between the coils. *(b):* feedback connecting the amplifier output to its inverting input, as in the prototype system. Here, however, the feedback resistor is thermally anchored to the coldest cryogenic stage, keeping it at sub-kelvin temperatures to reduce its Johnson noise contribution.

addressed.

The first of these is a feedback topology which connects the FET output to the transformer primary coil (shown in Figure 4.5a). This is advantageous, as a connection here acts as a virtual ground, shorting out leakage inductance which arises due to imperfect transformer coupling (see 4.3). In this configuration, the system transimpedance is given by $\frac{R_f}{(NA_0)^{-1}+1}$ and its input impedance by $\frac{R_f}{NA_0+1}$. However, connecting the amplifier's output to the transformer primary coil requires the use of lengthy wires inside the feedback loop, which poses a practical problem as discussed below.

Secondly, an attempt was made to improve the noise performance of the system by reducing the contribution from the feedback resistor, R_f. R_f is a resistive element which produces significant Johnson noise, and is a major contributor to the noise of the readout system as a whole (see Figure 3.3a).

The noise current the resistor produces is proportional to the square root of its temperature, so in an ideal system, R_f should be kept as cold as possible to minimize its contribution and improve the system's sensitivity.

Implementing this, however, presented practical challenges. To cool the feedback resistor, it must be thermally connected to the coldest cryogenic stage, which is physically separated by 10-20cm from the 4K stage on which the FET amplifier operates. This is best achieved by anchoring R_f to the sub-kelvin stage, requiring longer wire connections to the amplifier either to allow the resistor to be attached directly to the stage, or to avoid transmitting the amplifier's waste heat over a thermal link such as copper braid. To avoid these wires acting as an antenna, they are twisted together, reducing pick-up of ambient fields. Under testing, however, it was found that capacitive coupling between these twisted wires bypassed the feedback resistor to an extent that made it unusable over most of the 1 to 6 MHz bandwidth. Further difficulty arose from the lengths of the wires themselves. Negative feedback relies on a 180^o phase shift between the connected input and output signals, with a margin of 45^o after accounting for the 90^o phase shift of the amplifier beyond its first pole. To keep within these limits, the signal delay induced by the wire lengths in the feedback loop cannot exceed $^1/_8$ of the wavelength for frequencies up to the system's unity loop gain frequency (100MHz for the FET used in the prototype). Wire lengths must therefore be kept sufficiently short to maintain negative feedback up to 100MHz – a maximum loop length of 25cm (see Appendix D for derivation). This was on the edge of what was achievable in the cryogenic system used for testing, and resulted in additional thermal loading on the sub-kelvin stages. Due to these challenges, this arrangement was not implemented in the final prototype.

Of the avenues described above which were explored during the development of the prototype system, some were shown to be unsuitable, and though others held promise, practical constraints on the transformer turns ratio and feedback temperature led to the construction of the prototype system with $R_f = 10\text{k}\Omega$ and $N = 50$, which is intended to act as a proof-of-concept demonstration for a transformer-coupled FET amplifier-based readout architecture.

Chapter 5

Testing and Performance

In this chapter, the experimental setup and procedures involved in the characterization of the prototype system are described, as well as its performance under test in terms of transimpedance and noise.

5.1 Cryogenic setup

The prototype transformer-coupled system is installed for operation inside a multi-stage cryogenic refrigerator (Figure 5.1a and 5.1b), which allows its various components to operate at different temperatures (as in Figure 5.2). Biasing currents are supplied by room temperature digital electronics [27], which are transported into the cryostat and delivered to the multiplexed bolometers on the coldest cryogenic stage (~300mK) via specially-designed wire harnesses with careful heatsinking (part of this system is shown in Figure

(a)

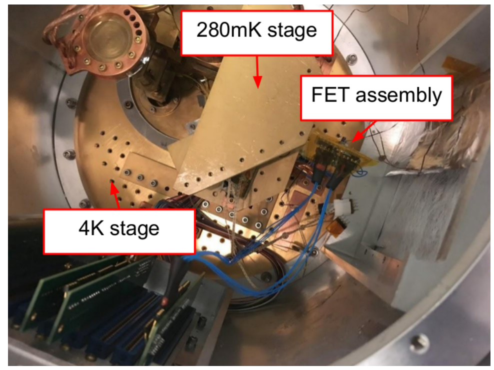

(b)

Figure 5.1: *(a):* cryogenic refrigerator (*cryostat*) inside which the prototype is installed for testing. A Cryomech PT410 [34] pulse tube cooler serves to bring the main stage to 4K, while a Simon Chase 4He-3He-3He adsorption fridge [35] provides additional cooling for 1.5K, 400mK, and 280mK stages. The cryostat is operated inside of an RF-isolating chamber, to reduce contamination from environmental signals. *(b):* view inside the cryostat. Sub-kelvin stages are stacked vertically with the topmost the coldest, and thermally isolated from each other and from the 4K stage, at bottom. The FET amplifier is visible in profile in the right of the image, installed upright on the 4K stage.

3.2a; the rest is internal to the cryostat). The signal is then sent through the transformer to the GaAs FET amplifier (Figure 3.2b) on the 4K cryogenic stage, and then back out of the cryostat to a secondary amplification stage at room temperature, which also supplies bias currents to the FET and is provided by Stahl Electronics [28]. The signal then is digitized and processed.

The temperature of the coldest cryogenic stage may be controlled in isolation from the others. This allows warming or cooling specific components of the system, while maintaining others at constant temperature. This is useful in the testing process, as the thermal Johnson noise of resistors on the sub-

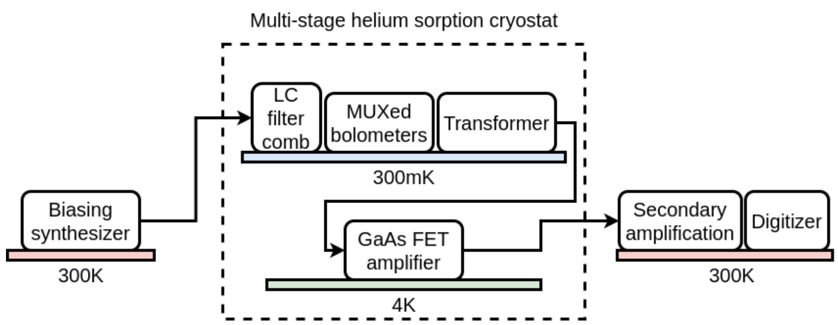

Figure 5.2: Block diagram of testing setup. The transformer-coupled protoype is installed within a multi-stage cryogenic refrigerator *(encircled by dotted line)*, while room temperature electronics (300K) provide auxiliary amplification, biasing currents, and output digitization. Inside the cryostat, the sub-kelvin stage (300mK) contains the fMUX filter comb and multiplexed bolometers, as well as the custom-built transformer. This stage is thermally isolated from the 4K stage, which hosts the amplifier, and its temperature can be controlled in a range from approximately 300mK up to 15K.

kelvin stage is used as a metric for the system's sensitivity. The cryostat is operated within an RF-isolating chamber, which attenuates ambient electromagnetic fields by 100dB, while the cryostat itself provides further isolation. Care must still be taken in the configuration of the signal input, output, and grounding to minimize environmental pickup and systemic feedback.

5.2 Performance

Though the readout system is designed with the eventual goal of operating bolometers, no light sensitivity is required in the initial testing and characterization phases, so for the purposes of simplicity, the TES bolometers which would typically be used with this readout architecture are replaced with 1 and 2Ω resistors, whose Johnson noise as a function of temperature is a useful test signal for the system's sensitivity.

The testing setup for the prototype transformer-coupled system is depicted in Figure 5.2. Inside the multi-stage cryogenic refrigerator, the biasing impedance (50mΩ), filter comb, resistors standing in for bolometers, and transformer (turns ratio $N = 50$) are installed on the sub-kelvin stage, with the FET amplifier on the 4K stage running in a current follower configuration with feedback resistor, $R_f = 10\text{k}\Omega$. The only active component in the system is the FET which dissipates approximately 28mW, a load which is easily handled by the large ($\sim$ 1W) cooling power of the main 4K stage, while thermal load on the ultra-cold stage (cooling power $\sim \mu$W) is kept minimal by use of exclusively passive components and superconducting connections were possible – the only dissipative component of the readout system which resides on the stage is the bias resistor, which might itself be replaced by an inductive or capacitive divider, as described in 4.1. The connection from the transformer secondary coil to the amplifier may be made arbitrarily long, further minimizing conductance of heat from the 4K stage.

5.2.1 Transimpedance

The transimpedance of a system is the ratio of its output voltage to its input current, $Z_{trans} = {}^{V_{out}}/_{I_{in}}$, and in this system depends on three parameters as $Z_{trans} = \frac{R_f}{N(A_0^{-1}+1)}$ (see Appendix A): the amplifier feedback resistance R_f, its open-loop gain A_0, and the transformer turns ratio N.

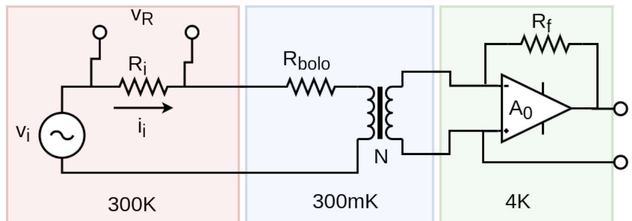

Figure 5.3: The prototype system with bias impedance removed. This allows the total system input current, i_i, to be computed by measuring the voltage across a test resistance, R_i, external to the cryostat. The system transimpedance can then be measured by comparing the system output voltage to the recorded input current. For ease of construction, this test is done with the system in a single-channel configuration, as in Figure 5.6.

In this readout architecture, the bolometers and system input are in parallel with a bias impedance, which sets the voltage across these elements, but also diverts some of the measureable input current away from the rest of the system. To measure transimpedance, in a seperate cryogenic run, the bias impedance is removed, to allow direct measurement of the system input current (depicted in Figure 5.3). As the factors which determine the transimpedance are located after the detectors on the signal path, this change is not expected to affect the transimpedance of the overall system. The system output voltage may then be directly measured along with the input current, which is computed as $i_i = {}^{v_R}/_{R_i}$ (where R_i is the value of the input resistor as shown in Figure 5.3), and these two compared to find a value of $Z_{trans} = 267 \pm 2\Omega$.

The predicted value for the transformer-coupled system, based on the circuit parameters, is $\sim 200\Omega$. The 30% higher measured value is consistent across repeated measurements, and may be due to capacitive coupling between windings on the secondary coil of the transformer, lowering the effective N from the counted value and thereby raising the system Z_{trans}. This effect may be investigated in future by characterization of self-resonances in the transformer, in particular of the secondary coil, which indicate the presence and magnitude of intra-winding capacitance.

5.2.2 Noise

When run without true bolometers in place, there are two main sources of noise in the prototype transformer-coupled system. The first is contributed by the system's amplification stages and resistive elements (such as the feedback resistor) which are not on the sub-kelvin stage, and is referred to the transformer primary loop as a current noise by Equation 3.4. This noise, generally termed *readout noise*, is independent of the temperature of the ultracold stages, and is measured to be to be $\lesssim 16\text{pA}/\sqrt{\text{Hz}}$, which, within the bounds of the uncertainty on system parameters such as the transimpedance, is within expectation (see Appendix A for more detail).

The other key source of noise in the prototype circuit is the Johnson noise produced by the multiplexed resistors, which stand in for the detectors on the coldest cryogenic stage. This noise is dependent on their temperature and on the impedance of the transformer primary loop (which is a sum of the values of the resistors themselves, the bias impedance, inductive impedances of the superconducting striplines which connect the filter comb to the loop, and

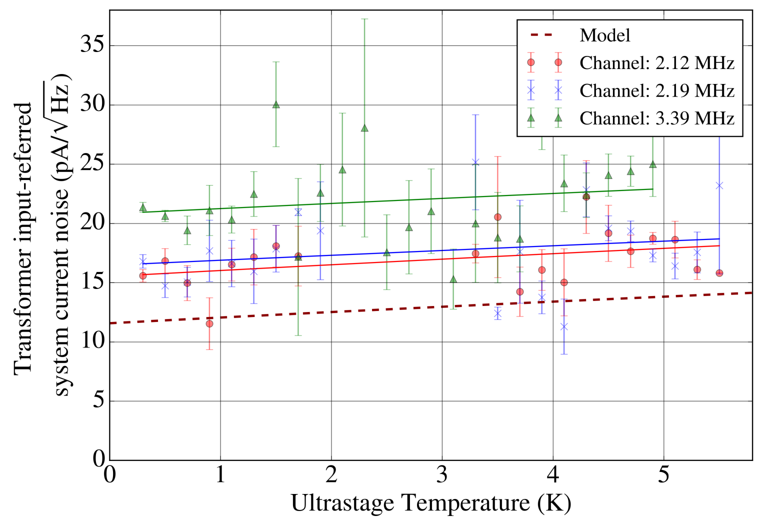

Figure 5.4: Total system voltage noise output, referred to the transformer primary loop as current noise, as a function of ultracold stage temperature, at low temperature for three channels, with overlaid fits (solid lines) for a quadratic sum of predicted resistor Johnson noise and temperature-independent system readout noise. These channels were selected for measurement at random and are assumed to be representative of of the remaining channels. The slope of the fit is in agreement with the predicted temperature dependence (dashed line), though to low significance at these low temperatures.

the primary-referred input impedance of the FET in feedback configuration; $\sim 1.4\Omega$ at 1MHz). This noise plays a similar role to that of a sky signal in the system, and at $3\mathrm{pA}/\sqrt{\mathrm{Hz}}$ for a 300mK 1Ω resistor, is a factor of several smaller than the expected photon noise of a system observing the sky. As such, the detection of a change in this noise with temperature would be a confirmation of the system's sensitivity.

The two noise contributions are uncorrelated, and so add in quadrature

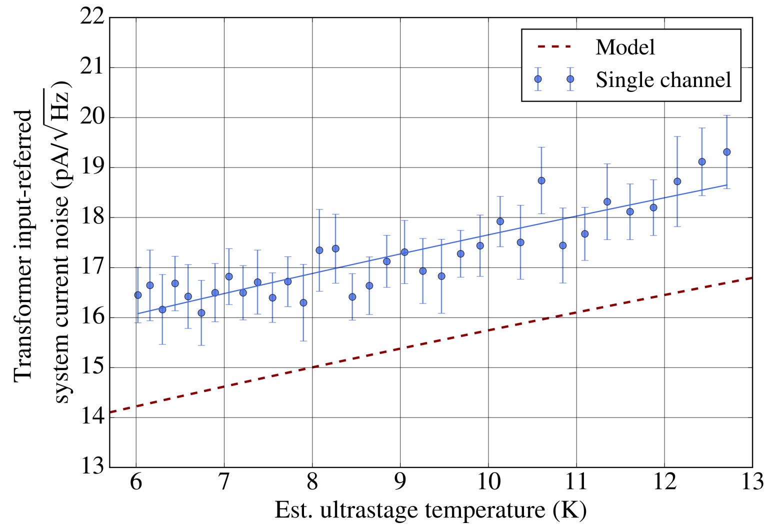

Figure 5.5: As in 5.4, but for a single-channel configuration of the transformer-coupled system (depicted in Figure 5.6), in which all superconducting elements have been removed (and which therefore operates only a single resistor channel). At these higher temperatures, the Johnson noise of the resistor has a visible impact on the total noise. EM interference from the temperature monitoring electronics was found to be an issue during this measurement, so data were taken without temperature monitoring equipment powered on; the ultra-cold stage temperature was instead estimated by repeating the identical sub-kelvin stage cycle with temperature monitoring systems powered on. This was done several times to ensure variations in the cycle's temperature versus time profile were small, so that the temperature of one cycle can be reliably estimated from the others.

as currents in the transformer primary loop, where the larger component will dominate. However, the temperature of the multiplexed resistors may be varied in effective isolation, as it is accompanied on the ultracold cryogenic stage only by the superconducting components such as the filter comb and by the small impedances of the bias and transformer coils, and the stage itself is thermally decoupled from the warmer cryogenic areas. Therefore, warming the ultracold stage will cause an increase in the magnitude of the resistor Johnson noise, while the readout noise contribution (from components kept at stable temperature) will remain constant. The increase in Johnson noise will increase the total input-referred current noise: for instance, the total at 300mK will be near 16pA/$\sqrt{\text{Hz}}$, while at 5K the resistor produces 11pA/$\sqrt{\text{Hz}}$, for a total at the transformer input of 19pA/$\sqrt{\text{Hz}}$. Though in this proof-of-concept system, the readout noise dominates in the low-temperature regime (below about 9K), the total noise in the primary loop will increase proportionally to the resistor temperatures below this, and this increase is observed as expected (see Fig 5.4, showing the total system noise referred to the transformer primary loop on three channels), though to low significance. This may be improved upon in future by constructing a system which more closely follows the optimization detailed in 3.4 (see also 6.2), but a more robust measurement of the Johnson noise may still be made using the existing prototype, by taking the stage to higher temperatures.

This presents a challenge for the multiplexed prototype as the fMUX architecture relies on the superconductivity of the niobium filter comb, which

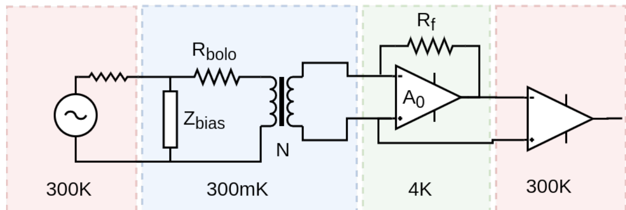

Figure 5.6: The single-channel configuration used to characterize the system at high temperature (> 9K). With the superconducting filter comb removed, the system operates a single channel – for testing purposes, a single 1Ω resistor standing in for a bolometer. The change in Johnson noise that this resistor produces as a function of its temperature is used as a test signal for the system's sensitivity.

transitions to normal resistance at 9.2K. For this high-temperature measurement, a single-channel alternate circuit as depicted in Figure 5.6 is used, which preserves the design of the prototype, though without any superconducting components, and so operates a single resistor channel. This allows it to be warmed well into a higher temperature regime, where the total noise is clearly seen to increase as a function of the resistor temperature, and the Johnson noise dominates (Figure 5.5).

Demonstrating its sensitivity to pA/$\sqrt{\text{Hz}}$-scale signals and with a measured transimpedance of 267 ±2Ω, an input impedance of $\sim$ 0.2Ω, and a readout noise level of 16 ±3pA/$\sqrt{\text{Hz}}$, the prototype provides proof-of-concept that this readout architecture, while not yet meeting the theoretical performance standards of SQUID-based systems, is feasible across a bandwidth of several MHz. This represents a significant milestone in demonstrating the viability of future fMUX systems which are not reliant on SQUIDs.

Chapter 6

Discussion

In this concluding chapter, the performance of the prototype system is contextualized alongside other existing systems and the predicted performance of an optimized transformer-coupled architecture.

6.1 Performance overview

Noise contributed by a readout system should not significantly degrade an instrument's sensitivity. A convenient gauge of this is to compare the noise of the readout system to the total of the phonon and photon noise through a typical detector, which is a noise that cannot be further reduced for a system operating TES detectors. In the example system described in Table 1.1, this noise has an equivalent power (NEP) of $60\mathrm{aW}/\sqrt{\mathrm{Hz}}$, which, for our detector parameters, corresponds to a current of $26\mathrm{pA}/\sqrt{\mathrm{Hz}}$. When the noise contribution of a readout system is added to this, the total will necessarily increase, but this increase should aim to be $\lesssim 5\%$.

In the prototype system described in the preceding chapter, the measured readout noise contribution of $16\pm3\mathrm{pA}/\sqrt{\mathrm{Hz}}$ does not meet this standard – rather, it constitutes a 17% increase on the detector noise. This is not wholly unexpected; while the framework for optimization as outlined in 3.4 was kept in mind during its design, its parameters were primarily chosen to facilitate construction, allowing it to serve as a preliminary proof-of-concept design for this style of readout architecture. To that end, the detection of the change in the Johnson noise of a 1Ω resistor, albeit at the high temperatures required by the limitations of the system, demonstrates a sensitivity which approaches that of experiments on the sky today [22], and indicates that further work is worth considering.

6.2 Predicted performance of an optimized system

While some gains in sensitivity may be achieved even without significantly altering the parameters of the prototype (for instance, keeping the FET's feedback resistor at sub-kelvin temperatures or by changing the second-stage amplifier to one designed for the purpose with a lower input voltage noise), the most significant improvement is to be made by building a new system with an optimized choice of components. As per 3.4, such a system would first select a maximum allowable input impedance, then choose corresponding values for the feedback resistance and transformer turns ratio, R_f and N respectively. The parameters and expected performance of an example system are shown below:

Prototype configuration		Optimized system	
Parameters	Demonstrated Performance	Parameters	Predicted Performance
$N = 50$	$Z_{in} \sim 0.2\Omega$	$N = 100$	$Z_{in} = 0.2\Omega$
$A_o = 20$	$Z_{trans} = 267 \pm 2\Omega$	$A_0 = 20$	$Z_{trans} = 520\Omega$
$R_f = 10k\Omega$	$i_{n,sys} = 16 \pm 3\text{pA}/\sqrt{\text{Hz}}$	$R_f = 55\text{k}\Omega$, $T_{Rf} < 0.4K$	$i_{n,sys} \lesssim 5\text{pA}/\sqrt{\text{Hz}}$

Table 6.1: Table comparing the measured performance of the transformer-coupled prototype with that of a parameter-optimized system. The input impedance, Z_{in}, is chosen to be 0.2Ω (small enough for operation with 1Ω bolometers), and the turns ratio, N, and feedback resistance, R_f, are then determined according to 3.4 to be 100 and $55\text{k}\Omega$, respectively. This sets the system transimpedance as 520 Ω, and the predicted total input-referred readout current noise to be $\lesssim 5$ pA/$\sqrt{\text{Hz}}$, assuming R_f, the dominant noise source in this system, is kept at or below 0.4K.

Constructing such a system might involve allowing additional flexibility in other design aspects. For example, a larger transformer core size would facilitate a higher turn count, or the modification of the readout layout to support the use of multiple cascaded cores. In the case of implementing this architecture on the scale of a modern on-sky experiment, these cores could be machine-wound. The regularity of mechanical production would address systematic issues in transformer characteristics, such as varied magnetic coupling and capacitive or inductive strays, which are serious concerns when handwinding. The predictability of wire placement on the core would allow better estimation in advance of the transformer properties, including strays. Further, a set of machine-wound cores would be near identical, allowing just one to be characterized and this characterization applied to the rest.

The transformer-coupled amplifier readout architecture uses simple components to achieve a wide linear range and streamlined operation. It reduces both wiring and operational complexity by removing the need for nulling configurations and eliminating SQUID tuning, and allows arbitrarily long connections from the coldest cryogenic stages to room temperature, further reducing thermal conduction to sensitive areas and allowing more flexibility in layout. The prototype configuration approaches the demonstrated performance of current on-sky experiments, and provides proof-of-concept that with the application of the changes outlined in Table 6.1, its performance may match or exceed that of existing SQUID-based fMUX systems.

Appendices

Appendix A

Derivations

A.1 Transformer-coupled system relations

This appendix details the process of deriving analytic expressions for system transimpedance, Z_{trans}, and input impedance, Z_{in}. They simplify the system

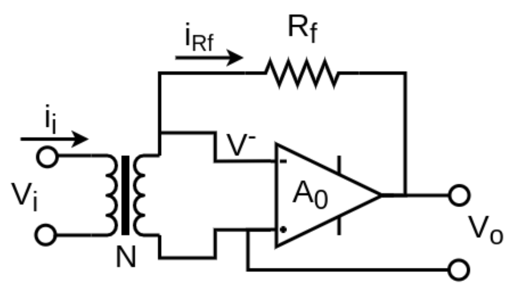

Figure A.1: Diagram of the transformer-coupled amplifier system, with relevant elements labelled for derivation of the analytical expressions of transimpedance and input impedance. Components are treated as ideal for simplicity. The input current, i_i, comes from the multiplexed bolometers, and the output voltage, v_o, goes to the secondary amplification stages.

by treating its components as ideal.

The transimpedance is the ratio of the system output voltage to its input current, $^{v_o}/_{i_i}$. For an amplifier, $v_o = -A_0 v^-$; with feedback, $v_o = v^- - i_{Rf} R_f$ is also true. Its input impedance is taken to be infinite and so diverts no current. Across a transformer, voltage is multiplied and current is divided by the turns ratio, N. So:

$$\begin{aligned} \frac{-v_o}{A_0} &= v_o + i_{Rf} R_f \\ v_o(\frac{1}{A_0} + 1) &= -i_{Rf} R_f \\ \frac{v_o}{i_{Rf}} &= \frac{R_f}{\frac{1}{A_0} + 1} \\ Z_{trans} = \frac{v_o}{i_i} &= \frac{R_f}{N(\frac{1}{A_0} + 1)} \end{aligned} \tag{A.1}$$

Similarly, for the input impedance:

$$\begin{aligned} -A_0 v^- &= v^- - i_{Rf} R_f \\ v^-(A_0 + 1) &= i_{Rf} R_f \\ \frac{v^-}{i_{Rf}} &= \frac{R_f}{A_0 + 1} \\ Z_{in} = \frac{v_i}{i_i} &= \frac{R_f}{N^2(A_0 + 1)} \end{aligned} \tag{A.2}$$

A.2 Input-referred noise contributions

The input voltage noise of the KC05d FET, $v_{n,FET}$, is first referred as a voltage to the amplifier output by its closed-loop gain, $\frac{R_f}{R_{bolo}N^2}$ (with R_{bolo} the bolometer resistance), then referred back to the transformer primary by dividing by the transimpedance of the transformer-coupled system:

$$i_{n,FET,v_n} = v_{n,FET}\frac{R_f}{R_{bolo}N^2}\frac{1}{Z_{trans}} = v_{n,FET}\frac{A_0^{-1}+1}{R_{bolo}N} \tag{A.3}$$

The input current noise of the KC05d FET, $i_{n,FET}$, follows a similar logic, being first referred to the amplifier output as a voltage by its transimpedance, then back to the transformer primary. This reduces to the form of the basic transformer current relation:

$$i_{n,FET,i_n} = i_{n,FET}\frac{R_f}{A_0^{-1}+1}\frac{1}{Z_{trans}} = i_{n,FET}N \tag{A.4}$$

Johnson noise from the feedback resistor presents as a voltage at the amplifier output, and is then referred to the transformer primary by dividing by the system transimpedance:

$$i_{n,R_f} = \frac{\sqrt{4k_BTR_f}}{Z_{trans}} = \sqrt{\frac{4k_BT}{R_f}}N(A_0^{-1}+1) \tag{A.5}$$

And likewise for the input voltage noise of secondary amplification stages:

$$i_{n,aux,v_n} = \frac{v_{n,aux}}{Z_{trans}} = v_{n,aux}\frac{N(A_0^{-1}+1)}{R_f} \tag{A.6}$$

Additional noise sources not listed here include Johnson noise of the bias resistor (several factors smaller than that of the 1Ω resistors which stand in for bolometers during testing), and Johnson noise from resistors on the signal input line (reduced by the bias resistor to be negligible in the transformer primary loop).

Adding these in quadrature gives the total estimated input-referred readout noise for the system. Due to the uncertainty on measured system values versus those computed based on constructed system parameters (for instance, the 30% discrepancy between the measured and predicted transimpedance), the expected noise value ranges between 11pA/$\sqrt{\text{Hz}}$ and 15pA/$\sqrt{\text{Hz}}$, for a system in perfect ambient RF isolation.

Appendix B

Transformer measurements

In pursuit of the ideal combination of turn counts and coupling, multiple cores were wound. The simplest way to achieve a high turns ratio is to use a single-turn primary. However, with the 70nH/turn^2 core, generally at least two turns are necessary for successful transformer operation (see Appendix C). Further increasing the number of turns on the primary was found in general to increase the coupling of the transformer.

A representative example of this was a core that was wound with 240 turns on its secondary, near the upper limit of what was able to physically fit on the small cores tested when using wire of a manageable gauge, even employing a multi-layered wrapping strategy (the highest achieved was 277, but the wrapping became so cramped and chaotic that abundant stray capacitance and poor coupling resulted in disappointing performance). Its coupling was then measured for 2, 4, and 9 turns on its primary, for turns ratios 120, 60, and 27, respectively. The coupling was found to increase from $k = 0.73$ for $N = 120$, to 0.82 for $N = 60$, to 0.89 for $N = 27$. While the latter coupling is desirable, the number of primary turns required to achieve it reduces the turns ratio to an unuseably low number, despite the high turn count on the secondary.

Based on these trials, we expect that relaxing the size constraint on the core will allow better transformer performance, as it will allow the placement of higher turn counts on both primary and secondary, allowing both high N and k.

Appendix C

Transformer minimum primary inductance

The primary inductance required for an effective tranformer may be considered for simplicity (for a more complete treatment of operating principles of transformers, see, for example, [36] or [37]) to be a function of the desired minimum operating frequency and its intended load impedance. The logic behind this is most easily demonstrated by comparing a simple transformer to an equivalent circuit, as in Figure C.1.

The ideal transformer in Figure C.1a may be represented by the parallel RL circuit in Figure C.1b by referring its load impedance, $R1$, across to its primary coil, such that $R2 = {}^{R1}/_{N^2}$, where N is the transformer turns ratio (which in this case, is 1). In the circuit in Fig. C.1b, it can be seen that current arriving at the transformer will be split between the two branches

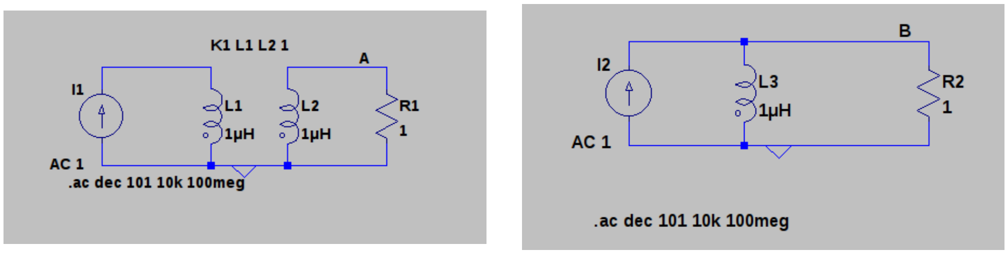

(a) (b)

Figure C.1: *(a):* simulation of an ideal 1:1 transformer with a 1Ω load. *(b):* an equivalent circuit for the same transformer, with the load resistor referred to the primary coil. Points A and B are equivalent, and the voltage here may be considered the output voltage of the transformer.

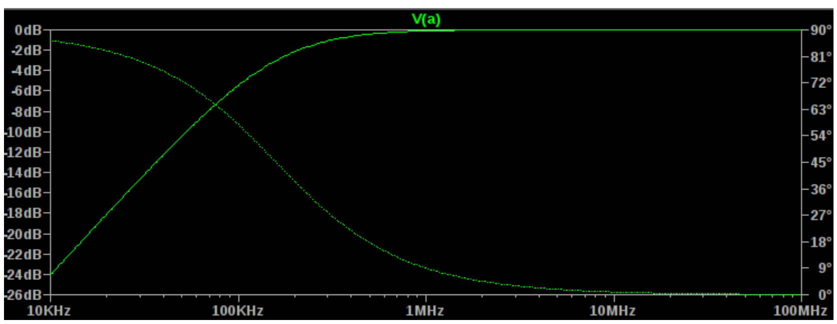

Figure C.2: Simulated output voltage for the equivalent circuits in Figure C.1a and C.1b. The -3dB point is located at the frequency at which the impedance of the transformer primary coil is equal to that of the input-referred load impedance.

of the circuit, and the primary inductor (which in this equivalent circuit is labelled as $L3$) will shunt current away from the load, reducing the voltage as measured at point B. We see that this condition causes a drop in the transformer output voltage (at equivalent points A and B), as shown in Figure C.2.

With these examples in mind, the minimum primary coil inductance may now be set. In the simulations above, the transformer has a -3dB point at approximately 160kHz (as can be read from Fig. C.2), which represents the point at which half the input current is being shunted away from the transformer. A minimum operating condition might be preferred to be the point at which a smaller fraction, such as 20%, be shunted away. Therefore, at the desired minimum operating frequency, the primary coil impedance should be a factor of 5 greater than that of the primary-referred load.

Appendix D

Feedback loop stability

A physical constraint encountered while developing the prototype system was the allowable length of wire in the FET feedback loop. Having this wire be arbitrarily long would facilitate placement of the feedback resistor, R_f, on

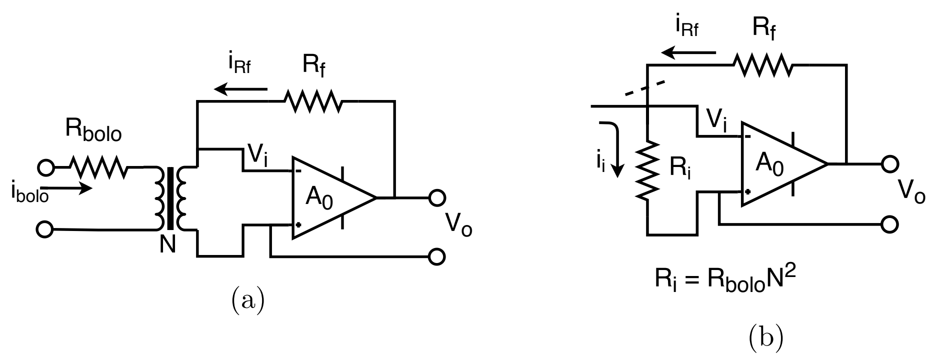

Figure D.1: The transformer-coupled system, demonstrating calculation of the loop gain. *(b)* is the equivalent circuit to *(a)*, with R_{bolo} referred to the transformer secondary as $R_i = R_{bolo}N^2$, and $i_{bolo} = i_iN$. The dashed line indicates where one might imagine cutting the circuit, to visualize the loop input and output currents.

the sub-kelvin cryogenic stage, reducing its thermal Johnson noise output (and that of the entire system). However, maintaining the stability of the amplifier's negative feedback places a limit on the length of the feedback loop to be 1/8 the wavelength of the signal at the frequency for which the loop gain is one. This corresponds to a 45^o phase shift, which when added to the 180^o of the amplifier's negative feedback and the additional 90^o beyond the amplifier's first pole, reaches a total phase shift of 315^o, taken as a rule of thumb to be the limit on negative feedback stability.

The loop gain is the ratio of the output current, i_{Rf}, from the feedback loop to the input current, i_i; these two currents are most easily visualized if the circuit in Figure D.1b were cut at the dashed line. In this system, this is calculated as follows:

$$\text{loopgain} = \frac{i_{Rf}}{i_i} = \frac{-A_0 v_i}{R_f}\frac{R_{bolo}N^2}{v_i} = -A_0\frac{R_{bolo}N^2}{R_f} \tag{D.1}$$

In the prototype system, with $R_{bolo} = 1$, $R_f = 10\text{k}\Omega$ and $N = 50$, this evaluates to $\frac{1}{4}A_0$. The value for the *open* loop gain, A_0, as a function of frequency, is provided by the manufacturer. Locating in the amplifier's datasheet the frequency at which $A_0 = 4$ (and therefore, the loop gain is 1), gives, by extrapolation, a unity gain frequency of 100MHz for the KC05d GaAs FET.

The wavelength of a 100MHz signal in a wire where the signal propagation speed is approximately 2/3 its speed in a vacuum, is $\lambda = 2$m. To maintain negative feedback, the phase difference between the returning current and the input current must be no more than 45^o, corresponding to $\frac{1}{8}\lambda = 25$cm of travel. The round-trip length of the feedback loop must therefore be no longer than this, to preserve stability in a negative feedback configuration.

Bibliography

[1] P. J. E. Peebles and J. T. Yu. Primeval adiabatic perturbation in an expanding universe. *Astrophys. J.*, 162:815–836, 1970. doi: 10.1086/150713.

[2] E. R. Harrison. Fluctuations at the threshold of classical cosmology. *Phys. Rev. D*, 1, 1970. doi: 10.1103/PhysRevD.1.2726.

[3] Y. B. Zeldovich. A hypothesis, unifying the structure and the entropy of the Universe. *Mon. Not. R. Astron. Soc.*, 160, 1972. doi: 10.1093/mnras/160.1.1P.

[4] R. A. Sunyaev. Fluctuations of the microwave background radiation. *The Large Scale Structure of the Universe, Proc.*, 1978.

[5] G. F. Smoot et al. Structure in the COBE differential microwave radiometer first-year maps. *Astrophys. J. Lett.*, 396, 1992. doi: 10.1086/186504.

[6] A. Melchiorri et al. A measurement of Omega from the North Amer-

ican test flight of Boomerang. *Astrophys. J.*, 536(2), 2000. doi: 10.1086/312744.

[7] S. Hanany et al. MAXIMA-1: A measurement of the cosmic microwave background anisotropy on angular scales of 10'-5deg. *Astrophys. J.*, 545 (1), 2000. doi: 10.1086/317322.

[8] G. Hinshaw et al. Three-year Wilkinson Microwave Anisotropy Probe (WMAP) observations temperature analysis. *Astrophys. J. Suppl. S.*, 170(2):288–334, 2007. doi: 10.1086/513698.

[9] T. Louis et al. The Atacama Cosmology Telescope: two-season ACTPol spectra and parameters. *J. Cosmol. Astropart. P.*, 2017(06), 2017. doi: 10.1088/1475-7516/2017/06/031.

[10] Planck Collaboration. Planck 2018 results. X. Constraints on inflation. *Astron. Astrophys.*, 2018. ISSN 0004-6361.

[11] R. Chown et al. Maps of the southern millimeter-wave sky from combined 2500 deg^2 SPT-SZ and *Planck* temperature data. *Astrophys. J. Suppl. S.*, 239(1), 2018. doi: 10.3847/1538-4365/aae694.

[12] W. Hu and M. White. A CMB polarization primer. *New Astron.*, 2, 1997. doi: 10.1016/S1384-1076(97)00022-5.

[13] T. Lanting. *Multiplexed readout of superconducting bolometers for cosmological observations.* PhD thesis, University of California, Berkeley, Department of Physics, 2003.

[14] D. Hanson et al. Detection of B-mode polarization in the cosmic microwave background with data from the South Pole Telescope. *Phys. Rev. Lett.*, 111, 2013. doi: 10.1103/PhysRevLett.111.141301.

[15] P. A. R. Ade et al. Measurement of the cosmic microwave background polarization lensing power spectrum with the POLARBEAR experiment. *Phys. Rev. Lett.*, 113, 2014. doi: 10.1103/PhysRevLett.113.021301.

[16] P. A. R. Ade et al. Constraints on primordial gravitational waves using *Planck*, WMAP, and new BICEP2/*Keck* observations through the 2015 season. *Phys. Rev. Lett.*, 121, 2018. doi: 10.1103/PhysRevLett.121.221301.

[17] M. A. Dobbs et al. Frequency multiplexed superconducting quantum interference device readout of large bolometer arrays for cosmic microwave background measurements. *Rev. Sci. Instrum.*, 83, 2012. doi: 10.1063/1.4737629.

[18] T. M. Lanting et al. Frequency-domain multiplexed readout of transition-edge sensor arrays with a superconducting quantum interference device. *Appl. Phys. Lett.*, 2005.

[19] A. Cukierman et al. Microwave multiplexing on the Keck Array. *J. Low Temp. Phys.*, 199, 2019. doi: 10.1007/s10909-019-02296-2.

[20] S. Henderson et al. Readout of two-kilopixel transition-edge sensor arrays for Advanced ACTPol. *Proc. SPIE 9914, Millimeter, Submillimeter, and Far-Infrared Detectors and Instrumentation for Astronomy VIII*, 2016. doi: 10.1117/12.2233895.

[21] T. de Haan. Recent advances in frequency-multiplexed TES readout: vastly reduced parasitics and an increase in multiplexing factor with subkelvin SQUIDs. *J. Low Temp. Phys.*, 199, 2020. doi: 10.1007/s10909-020-02403-8.

[22] A.N. Bender et al. Year two instrument status of the SPT-3G cosmic microwave background receiver. *Proc. SPIE 10708, Millimeter, Submillimeter, and Far-Infrared Detectors and Instrumentation for Astronomy IX*, 2018. doi: 10.1117/12.2312426.

[23] A. Suzuki et al. The POLARBEAR-2 and Simons Array experiments. *J. Low Temp. Phys*, 184, 2016. doi: 10.1007/s10909-015-1425-4.

[24] J. Clarke and A. I. Braginski. *The SQUID Handbook: Fundamentals and Technology of SQUIDs and SQUID Systems.* WileyVCH Verlag GmbH & Co. KGaA, 2004.

[25] J. Montgomery. Development of multiplexed bolometer readout electronics for mm-wave space astronomy. Master's thesis, McGill University, Department of Physics, 2015.

[26] B. A. Benson et al. SPT-3G: A next-generation cosmic microwave background polarization experiment on the South Pole telescope. *Proc. SPIE 9153, Millimeter, Submillimeter, and Far-Infrared Detectors and Instrumentation for Astronomy VII*, 2014. doi: 10.1117/12.2057305.

[27] K. Bandura et al. ICE: a scalable, low-cost FPGA-based telescope signal processing and networking system. *J. Astron. Instrum.*, 5(4), 2016. doi: 10.1142/S2251171716410051.

[28] Stahl Electronics. NexGen3 KC05d v.2014 cryogenic super low noise amplifier, 2016. URL `https://www.stahl-electronics.com/index.html`.

[29] C. Vergès. Preliminary design and test of a new readout system for transition-edge sensor bolometers. Technical report, McGill University, 2017.

[30] S. Gerber. Performance of high-frequency high-flux magnetic cores at cryogenic temperatures. Technical report, NASA, 2002.

[31] *Powder Cores: MPP, Hi-Flux, Super MSS (Sendust)*. Arnold Magnetics Limited, 2006.

[32] Rhombus Industries Inc. Testing inductance. URL `http://www.rhombus-ind.com/app-note/l-leak.pdf`.

[33] G. Barrere. Measuring transformer coupling factor k. URL `http://www.exality.com/files/Measuring/.../.pdf`.

[34] Cryomech Inc. PT410 Cryocoolers, 2020. URL https://www.cryomech.com/products/pt410/.

[35] Simon T. Chase. Chase research cryogenics, 2020 n.d. URL http://www.chasecryogenics.com/.

[36] D. Crosby. The Ideal Transformer. *IRE Trans. Circuit Theory*, 5(2): 145, 1958. doi: 10.1109/TCT.1958.1086447.

[37] M. Javid E. Brenner. *Analysis of Electric Circuits*. McGraw-Hill, 1959.